ARCHIVES OF ELECTRICAL ENGINEERING VOL. 66(4), pp. 681-692 (2017)

DOI 10.1515/aee-2017-0051

Comparative analysis of coaxial magnetocumulative generators

MIROSŁAW WOŁOSZYN, KAZIMIERZ JAKUBIUK,
PAWEL ZIMNY, DANIEL KOWALAK

Gdansk University of Technology
e-mail: miroslaw.woloszyn@pg.gda.pl

(Received: 23.10.2016, revised: 13.06.2017)

Abstract: This paper presents the results of a computer simulation of coaxial magnetocumulative current generators (MCGs). The simulation tests were carried out for different values of the internal diameter, length and speed of the deformation of the MGP element.

Key words: coaxial generator, magnetic field, magnetocumulative generator

1. Introduction

In order to study some very fast processes in scientific and technological applications, it is necessary to create a pulsed magnetic field or current pulses of very high magnitudes [3]. Such pulses are frequently created by means of magnetocumulative current generators (MCGs) [1, 2, 4]. The MCG multistage systems allow to create very short impulses of a magnetic field of several hundred teslas and currents of several hundred mega-amperes [1, 2, 4]. The magnetocumulation results from the magnetic field compression created in a system of electric conductors. The compression is caused by the change in the geometry of the conductor system obtained by means of explosive materials. The chemical energy in the MCG is transformed into electric energy. Since the magnetic flux ψ related to the conductor system remains constant and the geometry changes, compression of the magnetic field occurs. This will happen provided that the replacement inductance of the system decreases. Then the current magnitude increases according to the following equation [4]:

$$i = i_0 \frac{L_0}{L(t)}, \tag{1}$$

where: i_0, i are the currents in the system before and during the compression, respectively, and L_0, $L(t)$ are the system inductance, similarly before and during compression.

A cascade connection of several synchronised MCGs makes it possible to multiply the pulses generated by a single MCG. In practice, many various design solutions for MCGs are used [1, 2]. The major ones include: coaxial, spiral, plate, band and loop current generator design [1]. The simplest MCG coaxial design is based on two concentric tubes with current (Fig. 1).

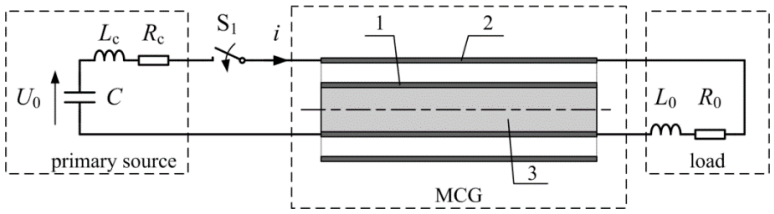

Fig. 1. The simplest coaxial MCG: 1 – internal tube, 2 – external tube, 3 – explosive material

The explosive material is placed inside the internal tube. As a result of the explosion the internal tube expands until there is no space between both tubes. The explosion in the coaxial generator can be triggered simultaneously along its whole length – in which case the radial compression occurs, or otherwise at the beginning of the system – in which case axial compression occurs (Fig. 2).

A comparative study of the effectiveness of two types of compression in a coaxial MCG was simulated. It was proved that in the MCG the impact of the skin effect on the generator's parameters could be ignored. Therefore, the effectiveness of a coaxial MCG can be studied with the use of a replacement circuit design taking into account only the change of inductance resulting from the geometry change of the generator. Based on the achieved simplified model of a coaxial MCG, it is possible to determine the most favourable parameters to ensure its highest efficiency.

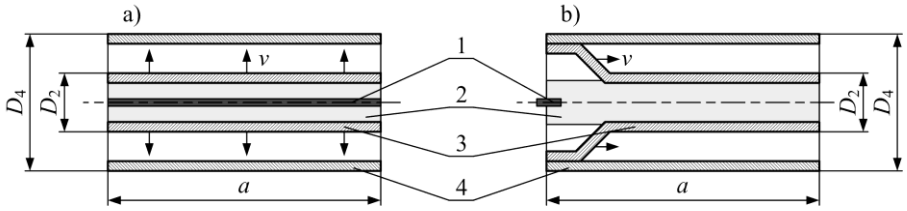

Fig. 2. Sketch of a coaxial MCG: a) the radial compression; b) the axial compression. D_4 is the diameter of the external tube, D_2 is the diameter of the internal tube: 1 – detonator, 2 – explosive material, 3 – internal tube, 4 – external tube

2. Skin effect analysis

The analysis of the coaxial MCG operation (Fig. 1) while taking into account the skin effect considerably complicates the calculations. The analysis based on a circuit model is

much simpler and often makes it possible to find analytical solutions, which allow to determine the optimum parameters of the generator.

The calculations of the influence of the skin effect and temperature on the circuit parameters (resistance and inductance) in the circuit model (Fig. 3) were conducted, taking into account the spatial distribution of the magnetic field. The calculations of the skin effect were performed for the period of time t_o from the connection of the capacitor to the time t_m when the explosion was initiated.

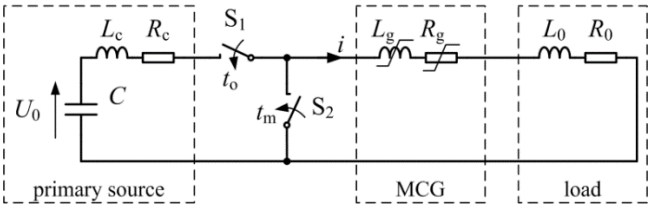

Fig. 3. The circuit model of the MCG. C, L_c, R_c are the capacity, inductance and resistance of the primary source, respectively, and L_g, R_g are the inductance and resistance of the MCG, respectively, and L_0, R_0 are the inductance and resistance of the load, respectively

In order to calculate the influence of the skin effect on the resistance and inductance of the generator, the 1D model was used to determine the distribution of the magnetic induction in the coaxial MCG:

$$\frac{\partial^2 B_k}{\partial r^2} + \frac{1}{r}\frac{\partial B_k}{\partial r} - \frac{B_k}{r^2} = \mu_0 \sigma_k \frac{\partial B_k}{\partial t}, \tag{2}$$

where: B_k is the angular component of the magnetic induction in the internal tube $k = 1$ and in the external tube $k = 2$, σ_k is the conductivity in the internal tube $k = 1$ and in the external tube $k = 2$, $\mu_0 = 4\pi 10^{-7}$ H/m is the magnetic permeability of the vacuum, r is the radial coordinate of the cylindrical coordinates system r, φ, z.

The solution of Equation (2) must fulfil the following boundary conditions:

$$\begin{aligned} B_1(0.5D_1, t) &= 0, \\ B_1(0.5D_2, t) &= \frac{\mu_0}{\pi D_2} i, \\ B_2(0.5D_3, t) &= \frac{\mu_0}{\pi D_3} i, \\ B_2(0.5D_4, t) &= 0, \end{aligned} \tag{3}$$

where: D_1, D_2 are the internal and external diameters of the internal tube, D_3, D_4 are the internal and external diameters of the external tube, i is the current in the MCG circuit.

Boundary conditions (3) are true until the beginning of the explosion, when the internal tube changes its diameter and both D_1 and D_2 are changed. It was assumed that the increase in

the radiuses depends on the constant velocity of the explosion and increases until both tubes are joined, that is when $D_2 = D_3$ (the movement is not analysed here). The system of Equation (2) with boundary conditions (3) with constant radiuses has a solution determined by a series of Bessel functions of the first and the second kind. The main difficulty is to determine eigen- values of the characteristic equation. It is mainly for this reason that a numerical solution using the finite difference method was chosen. The PSpice software was used to solve the system of equations describing the distribution of magnetic induction. Space discretisation was used and a system of ordinary differential equations in the number corresponding to the number of the mesh nodes was obtained (Fig. 4):

$$r_{k,n} = 0.5D_{k,n} + n\Delta_k\,, \tag{4}$$

where: $\Delta_1 = 0.5m_1^{-1}(D_2 - D_1)$ and $\Delta_2 = 0.5m_2^{-1}(D_4 - D_3)$ are the discretisation steps, m_1, m_2 are the numbers of divisions of the internal and external tubes, $D_{k,n}$ is the internal diameter of k-tube, n is the node number. As a result of approximation of Equation (2) by the finite difference method, it was received:

$$\frac{B_{k,n-1} - 2B_{k,n} + B_{n+1}}{\Delta_k^2} + \frac{B_{k,n+1} - B_{k,n-1}}{2r_{k,n}\Delta_k} - \frac{B_{k,n}}{r_{k,n}^2} = \mu_0\sigma_k \frac{\mathrm{d}B_{k,n}}{\mathrm{d}t}\,. \tag{5}$$

After transformations, Equation (5) becomes:

$$\frac{B_{k,n+1}}{\frac{2r_{k,n}}{\Delta_k}} - \frac{B_{k,n-1}}{\frac{2r_{k,n}}{\Delta_k}} - \gamma_k \frac{\mathrm{d}B_{k,n}}{\mathrm{d}t} - \frac{B_{k,n}}{\left(\frac{r_{k,n}}{\Delta_k}\right)^2} + \frac{B_{k,n-1} - B_{k,n}}{1} + \frac{B_{k,n+1} - B_{k,n}}{1} = 0\,, \tag{6}$$

where: $\gamma_k = \mu_0\sigma_k\Delta_k^2$ is the coefficient represented by capacity in an analogue circuit.

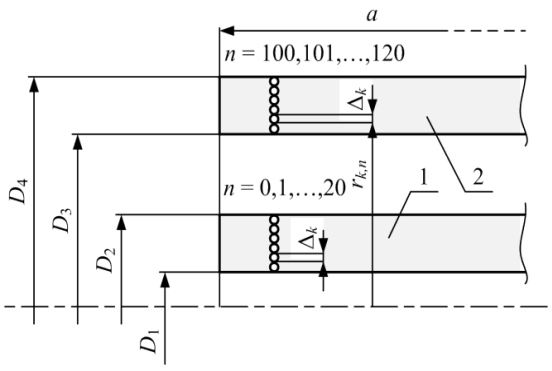

Fig. 4. Discretisation of the internal and external tube in 1D model: 1 – internal tube, 2 – external tube

The first two components of Equation (6) were replaced in the PSpice program with current generators. The coefficient γ_k represented by capacity in an analogue circuit is the third

component, and the current of the resistor of the value $(r_{k,n}/\Delta_k)^2$ is the fourth one. The last two components of Equation (6) are the currents in substitute resistors at a value of 1 Ω.

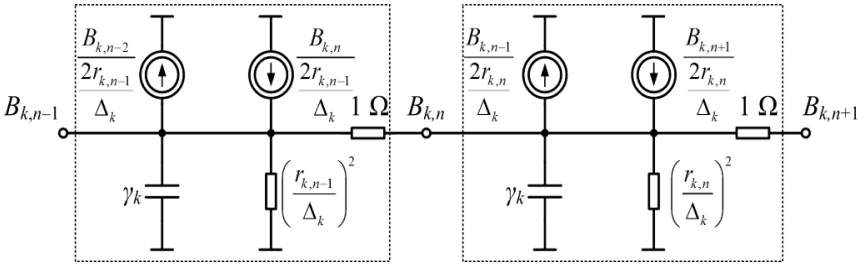

Fig. 5. Equivalent circuit of Equation (6) in node *n*

For this reason it was relatively easy to obtain equivalent circuits in the mesh nodes (Fig. 5) corresponding to the system of Equations (6) with boundary conditions (3), and to join them to the discharging circuit of the capacitor supplying the MCG. It allows to determine the current value i in the equivalent RLC circuit of the MCG powered from the capacitor. The equivalent RLC circuit is presented in Fig. 3 and has the parameters: $C = 100\ \mu$F, self-resistance of the capacitor and of the connecting wires is $R_c = 0.5$ mΩ, self-inductance of the capacitor is $L_c = 10$ nH, and the coil of the resistance of $R_0 = 1$ mΩ and inductance of $L_0 = 100$ nH is a load. A coaxial MCG was assumed, having the form of two concentric tubes of a length of $a = 200$ mm and an internal diameter of $D_1 = 20$ mm, $D_3 = 40$ mm for the internal and the external tube respectively. Copper tubes of conductivity $\sigma_1 = \sigma_2 = 5.7 \cdot 10^7$ S/m were used for the purpose of the test. The thickness of the walls is identical for both tubes and is 1 mm. The assumed initial voltage of the capacitor is 1 kV. The discharge of the capacitor is oscillatory, however, the calculations were performed only for the first half-wave, because it is the current value of the first crucial peak, after which the capacitor is switched off by the connector S_2 (Fig. 3). The current profile in the MCG, in the conditions of constant resistance and inductance of the cumulative generator, is presented in Fig. 6.

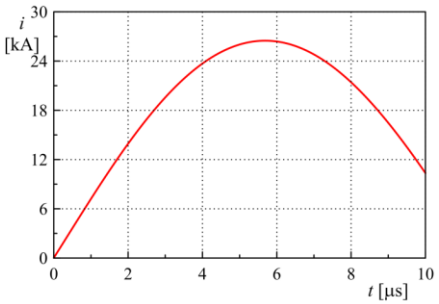

Fig. 6. Current profile in the MCG at constant resistance and inductance

Changes in resistance and inductance taking into account the spatial distribution of the electromagnetic field are presented in Fig. 7 and Fig. 8, respectively.

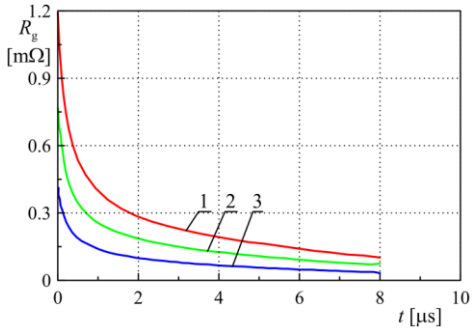

Fig. 7. Changes in coaxial MCG tubes' resistance taking into account the skin effect: 1 – resistance of both tubes, 2 – resistance of the internal tube, 3 – resistance of the external tube

The resistance of both tubes was calculated using the formula:

$$R_g = \frac{2\pi a}{i^2(t)}\left[\int_{0.5D_1}^{0.5D_2} \frac{j_1^2(r,t)}{\sigma_1} r\mathrm{d}r + \int_{0.5D_3}^{0.5D_4} \frac{j_2^2(r,t)}{\sigma_2} r\mathrm{d}r\right], \tag{7}$$

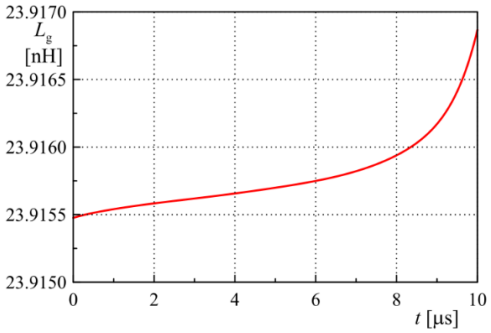

Fig. 8. Changes of inductance in the coaxial MCG taking into account the skin effect

The inductance was calculated using the formula:

$$L_g = \frac{\mu_0 a}{2\pi}\ln\left(\frac{D_3}{D_2}\right) + \frac{2\pi a}{i^2}\left\{\int_{0.5D_1}^{0.5D_2}\left[\frac{B_1^2(r,t)}{2\mu_0}\right] r\mathrm{d}r + \int_{0.5D_3}^{0.5D_4}\left[\frac{B_2^2(r,t)}{2\mu_0}\right] r\mathrm{d}r\right\}. \tag{8}$$

The inductance changes are practically of no significance, as can be seen in Fig. 8. The value of the MCG inductance depends on the magnetic energy cumulated in the space between the tubes and it is described by the first component of Equation (8). This fact was taken into consideration when calculating the current i in the MCG, taking into account the changes in the tubes' resistance resulting from the skin effect. In this case the calculated current waveform is practically identical as in Fig. 6.

As it was mentioned above, it is the value of the first current peak discharge and the time to reach the peak that is the most important for the operation of the MCG. The comparison of the current i at a constant resistance (Fig. 6) and at a variable resistance shows that the current peak values of 26.42 kA and 26.36 kA, respectively, are practically identical and occur at the same moment that is 5.63 μs. The analysis performed shows that the replacement coaxial MCG circuit can be assumed in the form of constant resistance calculated according to the formula:

$$R_g = \frac{a}{\pi}\left[\frac{4}{\sigma_1(D_2^2 - D_1^2)} + \frac{4}{\sigma_2(D_4^2 - D_3^2)}\right] \tag{9}$$

and the inductance is given by the first component in Equation (8).

Calculations of the MCG tubes temperature distribution resulting from the current i were performed, taking into account the changes of the conductivity resulting from the temperature increase described by the dependence:

$$\sigma_k = \frac{\sigma_{0k}}{1 + \alpha_k \theta_{k,n}}, \tag{10}$$

where: σ_{0k} is the initial electric conductivity in the internal tube ($k = 1$, $\sigma_{0k} = 5.7 \cdot 10^7$ Sm^{-1}), and ($k = 2$) in the external tube, α_k is the temperature conductivity coefficient ($\alpha_k = 0.004$ K^{-1}), $\theta_{k,n}$ is the temperature increase at mesh node n.

The temperature distribution was calculated assuming adiabatic heating of the generator's tubes, taking into account Formula (10) described by the equation:

$$\rho_k c_k \frac{\partial \theta_{k,n}}{\partial t} = \frac{j_{k,n}^2}{\sigma_{0k}}(1 + \alpha_k \theta_{k,n}), \tag{11}$$

where: ρ_k is the material density of the internal tube ($k = 1$) and of the external tube ($k = 2$, $\rho_k = 8930$ kg·m^{-3}), c_k is the specific heat capacity of the tube material ($c_k = 380$ J·kg^{-1}K^{-1}), $\theta_{k,n}$ is the temperature increase at mesh node n for the internal tube $k = 1$, $n = 0,1,...,20$ and for the external tube $k = 2$, $n = 100,101,...,120$, and $j_{k,n}$ is the current density at n node.

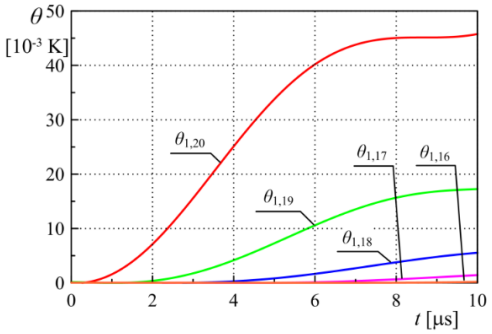

Fig. 9. Temperature rise distribution of the internal tube in node $r_n = 0.5D_1 + n\Delta_1$, where $\Delta_1 = 0.5(D_2 - D_1)/20$

The distribution of the temperature rise in the internal tube wall is presented in Fig. 9 and in the external one in Fig. 10, respectively.

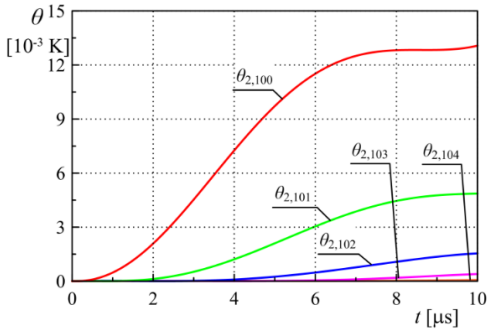

Fig. 10. Temperature rise distribution of the external tube in node $r_n = 0.5D_3 + (n - 100)\Delta_2$, where $\Delta_2 = 0.5(D_4 - D_3)/20$

The results obtained show that, for the period of time until the current peak of the capacitor's discharge, there was virtually no temperature increase, and therefore a constant resistance value can be assumed, which is described by Formula (9).

3. MCG circuit model

An MCG circuit model which takes into account the deformation of the internal tube and absence of the skin effect is shown in Fig. 3. At the time t_o the connector S_1 is closed. At the time t_m, when the current in the circuit voltage reaches the highest value, the explosive material is detonated and the connector S_2 is closed. Since that moment, the adopted coaxial MCG circuit model fulfils the equation [5]:

$$\frac{\partial \psi}{\partial t} + R_g i + L_0 \frac{\mathrm{d}i}{\mathrm{d}t} + R_0 i = 0 \,, \tag{12}$$

where: L_0, R_0 are the load inductance and resistance, respectively, R_g is the resistance of MCG, ψ is the magnetic flux.

The magnetic flux ψ in the MCG with radial compression (Fig. 2a) is calculated according to the following formula:

$$\psi = \frac{\mu_0 a}{2\pi} i \ln\left(\frac{D_3}{D_2 + 2vt}\right) \tag{13}$$

and with axial compression (Fig. 2b):

$$\psi = \frac{\mu_0 (a - vt)}{2\pi} i \ln\left(\frac{D_3}{D_2}\right) , \tag{14}$$

where: v is the detonation velocity.

The solution of Equation (12) for radial compression is:

$$i = I_o \frac{e^{-\frac{t}{T_a}}}{\left(1-\frac{vt}{a(1+\eta_L)}\right)^{1+(\eta_L-\eta_R)\frac{a}{vT_a}}}, \tag{15}$$

where:

$$\eta_R = \frac{R_0}{R_g}, \eta_L = \frac{L_0}{\frac{\mu_0 a}{2\pi}\ln\left(\frac{D_3}{D_2}\right)}, T_a = \frac{\frac{\mu_0 a}{2\pi}\ln\left(\frac{D_3}{D_2}\right)}{R_g}$$

and for axial compression:

$$i = \frac{I_o}{1-\eta_a \ln\left(1+\frac{2vt}{D_2}\right)}\left(\frac{1+\eta_a(0.5-\ln 2)-\eta_a\frac{2vt}{D_2}}{1+\eta_a(0.5-\ln 2)}\right)^{\frac{d}{v\eta_a T_b}}, \tag{16}$$

where:

$$\eta_a = \frac{\frac{\mu_0 a}{2\pi}}{\frac{\mu_0 a}{2\pi}\ln\left(\frac{D_3}{D_2}\right)+L_0}, \tag{17}$$

$$T_b = \frac{\frac{\mu_0 a}{2\pi}\ln\left(\frac{D_3}{D_2}\right)+L_0}{R_g+R_0}, \tag{18}$$

where: R_g = 0.5 mΩ, R_0 = 0.5 mΩ, L_0 = 10 nH, I_o = 10 kA.

For $t > t_m$, where t_m is the moment when both tubes are fully joined, the solution is described by the following formula:

$$i = i(t_m)e^{-\frac{t-t_m}{T_c}} \quad \text{for} \quad t > t_m, \tag{19}$$

where: $T_c = L_0/R_0$.

While performing the calculations for an MCG with axial compression, it was assumed that concatenation of the two tubes occurs along the axis, from the beginning to the end of the model, during the time $t_m = a/v$ (Fig. 2).

4. Results of computer simulations

For the purpose of performing calculations, two different constant detonation velocities v of the internal tube deformation were considered. Fig. 11 shows current i for both generators for $a = 0.2$ m, $D_3 = 4$ cm, $D_2 = 2$ cm. The peak voltages occur when both tubes are concatenating. Afterwards, the current disappears as a result of a transitional state in the circuit L_0R_0. Definitely, the highest voltages are obtained for the MCG with the radial compression. In the case of the axial compression with a deformation velocity of $v = 2$ km/s, a current increase does not occur. Fig. 12 shows a similar current i for both generators, but for the tubes' length $a = 0.1$ m. As Fig. 11 and Fig. 12 show, doubling the generator's length results in an increase of current peaks (they are from 1.5 to 2 times lower). If the generator is longer, the current is stronger. However, due to the difficulty in ensuring simultaneous concatenation of both MCG tubes, too long generators cannot be used. Fig. 13 and Fig. 14 show a similar current i for MCG generators as in Fig. 11 and Fig. 12, but for a twice lower dimensions D_3 and D_2. As Fig. 13 and Fig. 14 show, lowering the MCG diameters is not favourable due to lower peak current values.

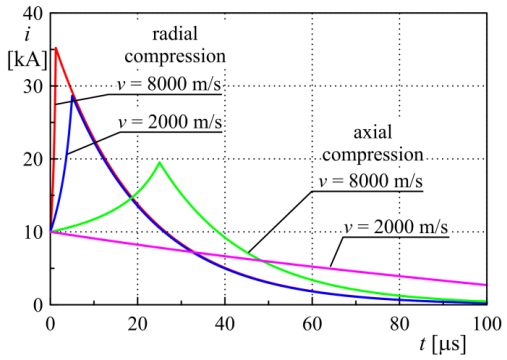

Fig. 11. Current i for an MCG with axial and radial compression for $a = 0.2$ m, $D_3 = 4$ cm, $D_2 = 2$ cm

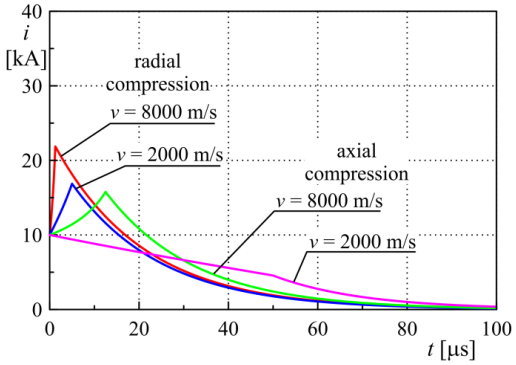

Fig. 12. Current i for an MCG with axial and radial compression for $a = 0.1$ m, $D_3 = 4$ cm, $D_2 = 2$ cm

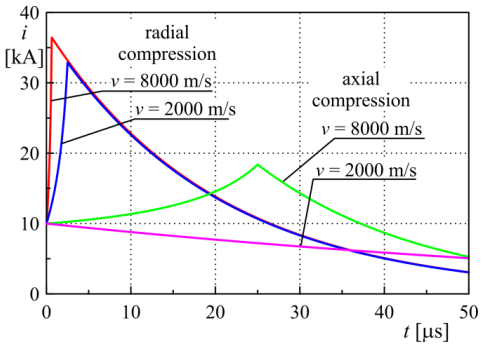

Fig. 13. Current i for an MCG with axial and radial compression for a = 0.2 m, D_3 = 2 cm, D_2 = 1 cm

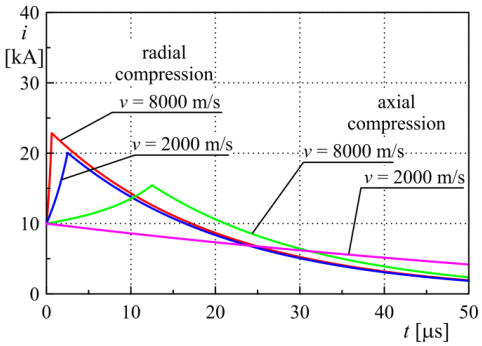

Fig. 14. Current i for an MCG with axial and radial compression for a = 0.1 m, D_3 = 2 cm, D_2 = 1 cm

5. Conclusions

The current amplification factor during magnetocumulation can be adopted as the efficiency of the MGC operation [1, 4]. Computer analysis of the two types of coaxial MCGs with the structure and parameters most frequently used in practice [1, 4] allows to draw the following conclusions:

1) A circuit model, which does not take into account the skin effect, can be used as a model for the analysis of the current amplification factor of the MCG.
2) A generator with radial compression is a more favourable solution because it allows to obtain a high current amplification factor at the level 3.5 (Fig. 11). The current amplification factor of the generator with axial compression is lower by about 50%.
3) There is a minimum velocity of the internal tube deformation, below which current increase cannot be obtained.
4) The current amplification factor of MCGs of greater length and with a greater both tubes' diameters is higher. However, both the length and the diameters' ratio are limited due to the technical conditions of the generator's operation.

Acknowledgements

The study was financed from the NCBiR (National Center for Research and Development) funds within the project no. DOB-1-1/1/PS/2014.

References

[1] Altgilbers L.L., Brown M.D.J., Grishnaev I. et al., *Magnetocumulative Generators*, foreword by Fowler C.M., Springer Verlag, New York (2000).
[2] Knoepfel G., *Pulsed High Magnetic Fields*, North-Holland Publishing Company, Amsterdam (1970).
[3] Knoepfel H.E., *Magnetic fields*. *A Comprehensive Theoretical Treatise for Practical Use*, John Wiley & Sons, New York, Chichester, Weinheim, Brisbane, Singapore, Toronto (2000).
[4] Neuber A.A., *Explosively Driven Pulsed Power*. *Helical Magnetic Flux Compression Generators*, Springer-Verlag, Berlin, Heidelberg (2005).
[5] Wołoszyn M., Jakubiuk K., Zimny P., *The coaxial magnetocumulative current generator*, Poznań University of Technology Academic Journal Electrical Engineering, no 85, pp. 53-59 (2016).